Magnetohydrodynamic Simulations of Self-Consistent Rotating Neutron Stars with Mixed Poloidal and Toroidal Magnetic Fields

Antonios Tsokaros,[1,*] Milton Ruiz,[1] Stuart L. Shapiro,[1,2] and Kōji Uryū[3]
[1]*Department of Physics, University of Illinois at Urbana-Champaign, Urbana, Illinois 61801, USA*
[2]*Department of Astronomy and NCSA, University of Illinois at Urbana-Champaign, Urbana, Illinois 61801, USA*
[3]*Department of Physics, University of the Ryukyus, Senbaru, Nishihara, Okinawa 903-0213, Japan*

(Received 29 October 2021; revised 21 December 2021; accepted 10 January 2022; published 8 February 2022)

We perform the first magnetohydrodynamic simulations in full general relativity of self-consistent rotating neutron stars (NSs) with ultrastrong mixed poloidal and toroidal magnetic fields. The initial uniformly rotating NS models are computed assuming perfect conductivity, stationarity, and axisymmetry. Although the specific geometry of the mixed field configuration can delay or accelerate the development of various instabilities known from analytic perturbative studies, all our models finally succumb to them. Differential rotation is developed spontaneously in the cores of our magnetars which, after sufficient time, is converted back to uniform rotation. The rapidly rotating magnetars show a significant amount of ejecta, which can be responsible for transient kilonova signatures. However, no highly collimated, helical magnetic fields or incipient jets, which are necessary for γ-ray bursts, arise at the poles of these magnetars by the time our simulations are terminated.

DOI: 10.1103/PhysRevLett.128.061101

Introduction.—Neutron stars are not only the densest objects in the Universe, but in some cases they possess a magnetic field billions of times larger than the strongest magnet on Earth. These so called magnetars [1–3] have magnetic fields that surpass the quantum electrodynamic threshold of 4×10^{13} G and are responsible for many exotic phenomena, such as vacuum birefringence, photon splitting, and the distortion of atoms (see Ref. [4] for a review). They are invoked in order to explain the large bursts of γ rays and x rays in soft-γ repeaters [5] or the related anomalous x-ray pulsars [6].

Magnetars are also naturally produced after the merger of two neutron stars (NSs) via the instigation of various magnetic instabilities such as the Kelvin-Helmholtz instability [7–11], the magnetorotational instability (MRI) [10,12–14], or magnetic winding [9,15,16]. Even if the two NSs that compose the binary system have magnetic fields of the order of $\sim10^{11}$ G, when they merge because of the aforementioned mechanisms the magnetic field reaches magnetar strengths and beyond on a dynamical timescale. This was first demonstrated with the very high resolution studies in Ref. [9,10] where an initial magnetic field of 10^{13} G was amplified to $\gtrsim10^{15}$ G, with local values reaching $\sim10^{17}$ G, 5 ms following merger. Similar results have been reported more recently in Ref. [17] where an even larger amplification was achieved. The existence of this ultrastrong magnetic field is one of the most crucial factors for the realization of multimessenger astronomy. According to our current understanding, the merger of the two NSs in event GW170817 [18] produced such a magnetar that was instrumental for the creation of the short γ-ray burst [19] (possibly following its delayed collapse), and the kilonova [20,21] that followed.

Despite the large amount of research in analytical and perturbative magnetohydrodynamics, self-consistent general relativistic solutions of the Einstein-Maxwell-Euler system are still in their infancy. In Ref. [22] self-consistent equilibria have been obtained with only poloidal magnetic field, while a different formalism was employed in Ref. [23,24] to obtain self-consistent equilibria with only toroidal magnetic fields. Other authors have explored such solutions in great detail [25–29] while in Ref. [30–32] solutions with mixed poloidal and toroidal magnetic fields were obtained with the price of greatly reducing the number of Einstein equations solved. On the other hand, equilibrium solutions are not necessarily stable, and indeed, the first general relativistic magnetohydrodynamic (MHD) simulations with either purely toroidal magnetic fields [33] or purely poloidal magnetic fields [34–37] confirmed the unstable nature of these solutions predicted decades ago [38–43]. In Ref. [34–37] the initial conditions were based on the self-consistent poloidal solutions of [22]. In all cases the Cowling approximation was used, i.e., the Einstein field equations were not evolved but only the MHD equations on the fixed initial background. In Ref. [33] the initial toroidal conditions were those of [23] and an axisymmetric general-relativistic magnetohydrodynamic (GRMHD) simulation was employed.

The stability of a pulsar magnetic field, as well as the recent results by NICER [44,45], demand a more sophisticated modelling of a NS magnetic field. As a first step we

TABLE I. The magnetar models evolved in this Letter. Columns are as follows: the model name, the polytropic index, the central rest-mass density in g/cm^3, the gravitational mass, the period, the ratio of polar to equatorial radii, the rotational kinetic energy, the total magnetic energy, the toroidal magnetic energy, the poloidal magnetic energy, the dynamical timescale $(1/\sqrt{\rho_0})$, and the Alfvén timescale. $|\mathcal{W}|$ denotes the gravitational energy, while the * denotes that this model collapses to a black hole. In our units $M = 1$ corresponds to ~ 5 μs.

Case	Γ	ρ_{0c} $(\times 10^{15})$	M	P/M	R_p/R_e	$\mathcal{T}/\|\mathcal{W}\|$ $(\times 10^{-2})$	$\mathcal{M}/\|\mathcal{W}\|(\times 10^{-2})$	$\mathcal{M}_{\rm tor}/\|\mathcal{W}\|$ $(\times 10^{-4})$	$\mathcal{M}_{\rm pol}/\|\mathcal{W}\|$ $(\times 10^{-2})$	t_d/M	t_A/M
$A1$	2	1.072	1.385	173.0	0.7	4.531	3.026	0	2.970	17	56
$A2$	2	1.072	1.366	169.3	0.7	4.871	1.632	7.863	1.525	18	70
$A3$	2	1.072	1.362	172.0	0.7	4.730	1.794	8.876	1.669	18	61
$A4$	2	1.072	1.359	175.3	0.7	4.568	1.983	8.707	1.852	18	47
$A5$	2	1.072	1.197	769.3	0.925	0.2612	1.709	7.492	1.632	20	45
$A6^*$	2	2.225	1.586	90.77	0.6	5.055	0.1624	0.5361	0.1504	11	126
$A7$	3	1.225	1.592	119.1	0.7	4.043	4.399	17.81	4.134	14	18

go beyond the previous works above by constructing rotating, magnetized equilibria with mixed ultrastrong poloidal and toroidal components and evolve them in full GRMHD in order to assess their evolutionary fate. Our initial data are constructed with the magnetized, rotating NS libraries of the COCAL code [46,47], where the *whole* set of the Einstein-Maxwell-Euler system is solved to construct models under the assumptions of perfect conductivity, stationarity, and axisymmetry. These models are then evolved using the Illinois GRMHD code [48] in full general relativity. The salient characteristics of our simulations are summarized in the Results section below, while details on the construction of the self-consistent models, as well as our choices for the simulations, are provided in Supplemental Material [49]. Here and throughout we adopt units of $G = c = M_\odot = 1$, unless otherwise noted.

Initial data.—We construct the initial magnetized equilibria, models $A1$–$A7$ in Table I by solving the Einstein equations, Maxwell's equations, and ideal MHD equations self-consistently under the assumptions of stationarity and axisymmetry. All of our models use a polytropic equation of state with $\Gamma = 2$, except the last model that has $\Gamma = 3$. Model $A6$ is supramassive [66], while all others are normal NSs. Models $A1$–$A4$ are rapidly rotating NSs with the same central density ρ_{0c} and polar to equatorial radius deformation R_p/R_e, but with the ratio of toroidal to poloidal B-field energies $\mathcal{M}_{\rm tor}/\mathcal{M}_{\rm tor}$ changed systematically. Model $A5$ is a slowly rotating NS whose parameters that determine the B fields are the same as in model $A4$. Model $A6$ is close to the mass-shedding limit curve and the maximum mass of unmagnetized, uniformly rotating equilibrium (to the left). Finally, model $A7$ is a moderately rotating normal NS. All magnetars have magnetic energy which is at most 4.4% of their gravitational potential energy. Most of this energy is poloidal in nature (expressions of how these energies are computed are given in Ref. [47]) since the toroidal magnetic field is confined to a region below the surface of the NS, therefore its volume is much smaller than the corresponding one for the poloidal field, which extends to infinity. However, the maximum values of the toroidal and the poloidal magnetic fields are of the same order. This can be seen in Fig. 1 where we plot various components of the magnetic field (toroidal is B^y) across the x and z axes. Vertical dashed lines signify the magnetar radii. In the last two columns of Table I we show the dynamical and Alfvén timescales ($t_A = R_e\sqrt{4\pi\rho_0}/B$, where B is the value of the magnetic field at the NS center) of our models. A more precise estimate of the Alfvén timescale based on the relativistic formula is given in Supplemental Material [49], and broadly agrees with the timescales of Table I. All models have been evolved for 10–20 Alfvén times, with the longest being magnetar $A7$ ($\sim 20 t_A$).

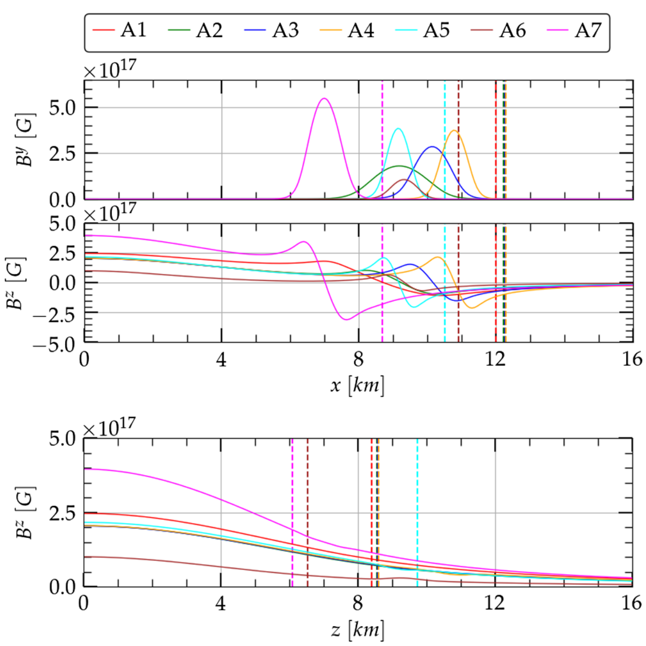

FIG. 1. Initial magnetic field strength along the x and z axes for all magnetars $A1$–$A7$, where z is the rotational axis. Vertical dashed lines show the corresponding NS radii. The toroidal magnetic field (B^y) is concentrated in a region below the NS surface. Note that the lines (radii) for $A1$–$A3$ closely overlap.

Evolutions.—Magnetars $A1$–$A7$ are evolved using the Illinois GRMHD moving-mesh-adaptive-refinement code (see, e.g., Ref. [48]) using the settings described in Ref. [65], and summarized in Supplemental Material [49]. In all our simulations we use high resolution, with the finest refinement level having $\Delta x_{\min} = 87$ m for the $\Gamma = 2$ models, having radii 10.5–12.3 km, and $\Delta x_{\min} = 72$ m for the $\Gamma = 3$ model, which has a radius of 8.7 km.

Results.—The behavior of our magnetized neutron stars can be broadly described by the following characteristics: (i) large radial density oscillations, especially for the rapidly rotating magnetars. (ii) Uniform rotation is destroyed in the core of the stars, which at instances becomes counterrotating. (iii) The NSs remain axisymmetric to a large degree. (iv) The toroidal magnetic field is the first to become unstable. (v) The timescale of the instability is longer for smaller toroidal magnetic field strengths, although the strength is comparable in all cases. Models with the strongest toroidal B field exhibit a density dip inside the star (as described in Ref. [47]), are the most unstable and develop a "gearlike" shape at the NS surface. (vi) All our models develop the "varicose" and "kink" instabilities [39–41].

In Fig. 2 we show 3D renderings of model $A2$ (top row) which has proven to be the most stable, and model $A7$ (bottom row) which has the strongest toroidal magnetic field at four different instances. Also in Fig. 3 along with the density profile we show the poloidal and toroidal field lines on the meridional and equatorial planes respectively at four instances for model $A2$. After approximately $\sim 10 t_A$ model $A2$ preserves broadly both its shape as well as the geometry of its toroidal and poloidal magnetic fields. In Fig. 2 green lines signify the combined poloidal and toroidal magnetic field while in Fig. 3 black field lines signify regions of strong magnetic field. On the other hand model $A7$ after $\sim 10 t_A$ exhibits turbulent motion on its surface, together with large density oscillations close to the surface and at $\pm 45°$ from the equatorial plane. By that time the toroidal geometry of the magnetic field is lost and the kink instability is fully developed. It has been suggested that the instability can trigger giant magnetar flares [3] and may be accompanied by a change in the mass quadrupole moment that can potentially lead to detectable gravitational waves [67,68]. In our simulations our stars preserve their general (hydrostatic) axisymmetry and we did not observe any significant nonaxisymmetric mode growth that can lead to appreciable gravitational wave emission, in accordance with [36,37,69].

Figure 4 shows the azimuthally averaged angular velocity $\bar{\Omega}(r) = 1/(2\pi) \int_0^{2\pi} u^\phi / u^t d\phi$ in the equator, plotted along the x axis, for models $A2$ (top panel) and model $A7$ (bottom panel) at six different instances. Although all our models initially are uniformly rotating, in a couple of dynamical timescales differential rotation arises in their core at distances within half their radii. One broad characteristic of this differential rotation is that it resembles the one found after the merger of two NSs [70–73]. In our simulations this behavior has developed spontaneously and is probably associated with the strong poloidal magnetic field. If the strength of the poloidal magnetic field is indeed responsible for the angular velocity drop at the center of the merger remnant (before uniform rotation is restored) that can have consequences in its evolution. A second characteristic is that the angular velocity in the core at various instances drops to zero and even takes negative values, which is reminiscent of the behavior found in analytical models [16]. Differential rotation generates toroidal Alfvén waves that convert kinetic energy into magnetic field and thermal [74] energy. Eventually, we expect that the differential rotation will be washed out and the star will come

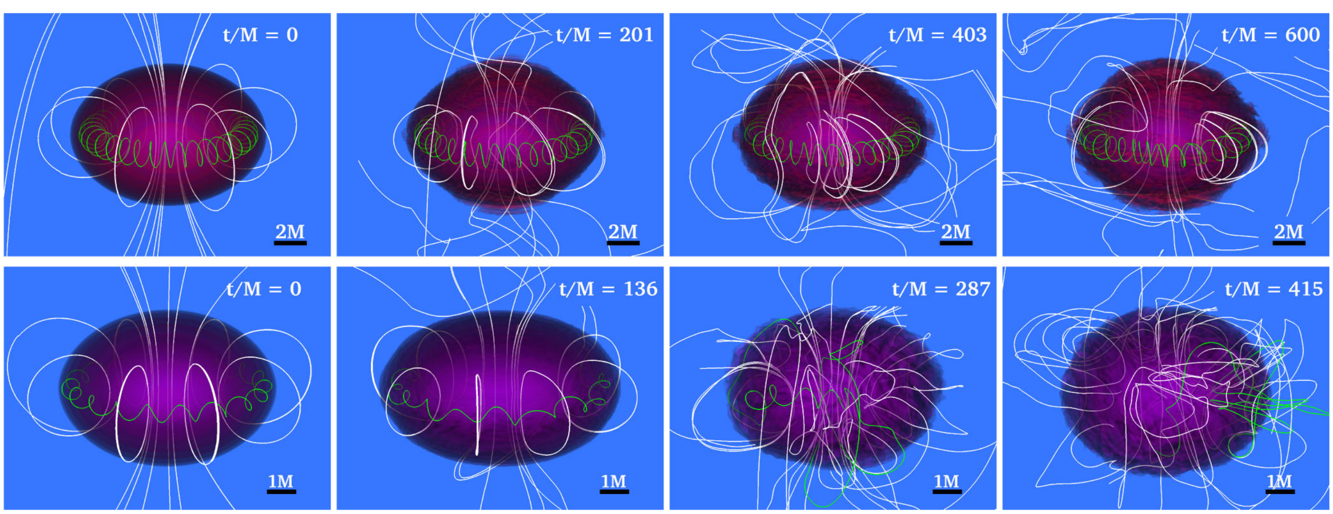

FIG. 2. Three-dimensional renderings of model $A2$ (top row) and $A7$ (bottom row) at four different instances of time. White lines show the poloidal field lines while green lines show a poloidal + toroidal one. The tighter the coil of the helix, the smaller the toroidal magnetic field. For model $A2$, $t = 600M \approx 9 t_A$, while for model $A7$, $t = 415M \approx 23 t_A$.

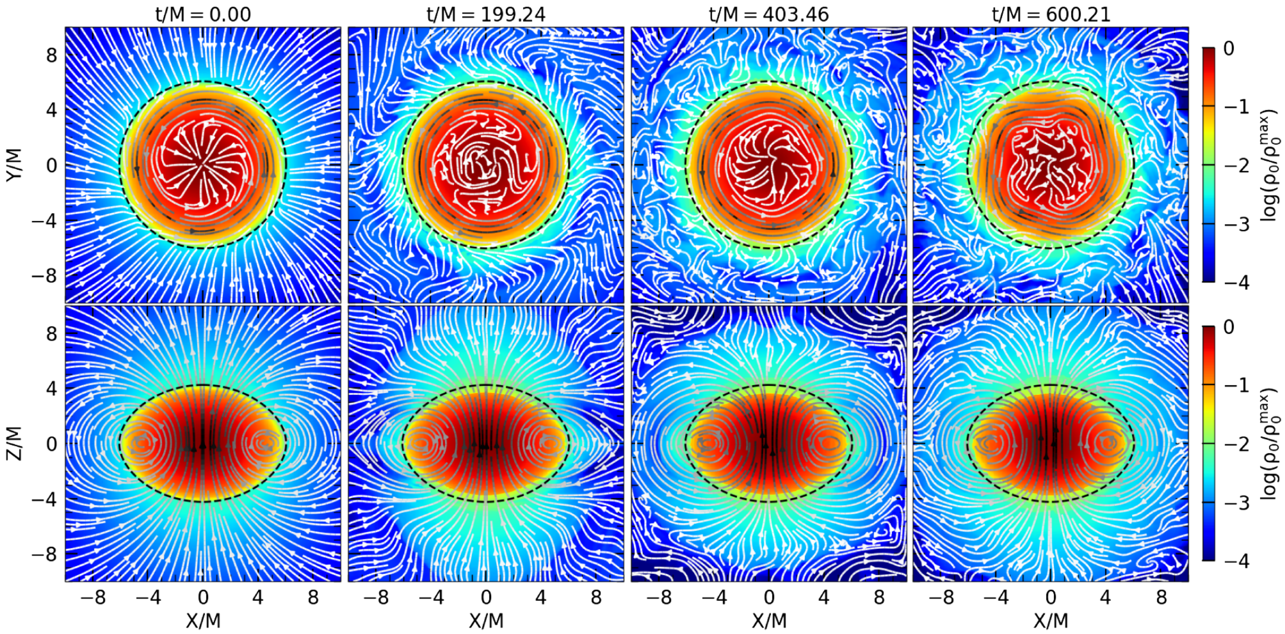

FIG. 3. Rest-mass density and magnetic field lines for model $A2$ on the equatorial and meridional planes at four time instances. Dark field lines signify a stronger magnetic field.

back to uniform rotation at the end due to the effective turbulent viscosity induced by MRI, as can be seen for model $A7$ in Fig. 4.

Models $A3$, $A4$, and $A5$ exhibit a dip in the density profile just below the NS surface due to the strength of the toroidal magnetic field. This phenomenon was first found in Ref. [47] in mixed poloidal and toroidal configurations. In our case it is more pronounced in model $A4$ in which the pressure becomes zero inside that magnetar, creating a toroidal electrovacuum region. These equilibria turn out to be the most unstable since the radial oscillations in conjunction with the "varicose" and "kink" instabilities destroy this electrovacuum on Alfvén timescales and create turbulentlike phenomena on the NS surface. The density profile of model $A2$, which was the most stable magnetar, had essentially no such density dip and therefore no hydrostatic pressure depletion below its surface.

The normalized maximum density of our magnetar solutions is plotted in Fig. 5 (top panel) where oscillations of $10\% - 30\%$ are visible. Note that the largest oscillations are present for the rapidly rotating magnetars $A1$–$A4$ and $A6$. However, the very slowly rotating model $A5$ and the moderately rotating model $A7$ exhibit oscillations of $\sim 10\%$. The large oscillations of model $A6$ are responsible for its collapse to a black hole, since the close proximity of this magnetar to the maximum supramassive limit [66] drives it to the unstable branch [75] (we have performed a resolution study to confirm this conclusion). In the scenario of a binary NS merger we expect that supramassive remnants close to the maximum mass limit will be similarly unstable.

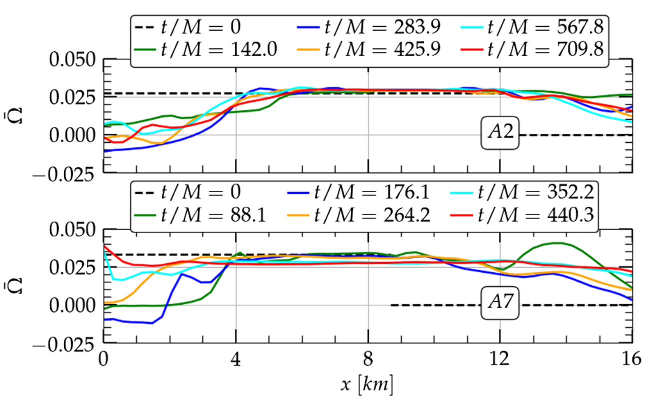

FIG. 4. Azimuthally averaged angular velocity in the equatorial plane inside the magnetars $A2$ (top panel) and $A7$ (bottom panel) at six instances.

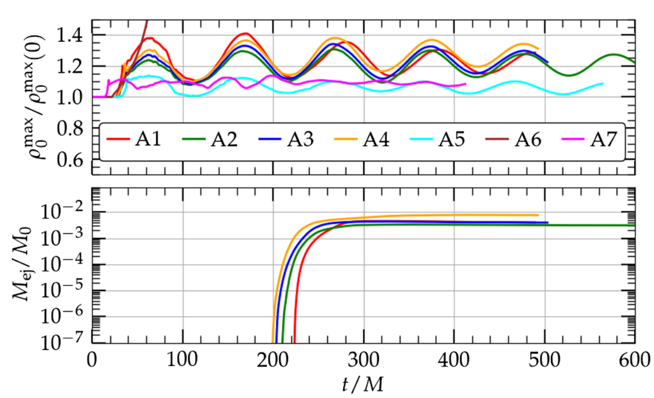

FIG. 5. Normalized maximum rest-mass density (top panel) and ejecta (bottom panel). Here $\rho_0^{\max}(0)$ is the initial maximum density and M_0 is the initial rest mass.

The timescale of the oscillations in Fig. 5 are of the order of an Alfvén timescale and are not present in the absence of the magnetic field. Indeed, if for the collapsing model $A6$ we reset the magnetic field to zero, it stays in a quasiequilibrium state and no collapse is triggered. In the bottom panel of Fig. 5 we plot the ejected material from our simulations. Note that detectable, transient kilonova signatures powered by radioactive decay of unstable elements formed by neutron-rich material are expected for ejecta masses $\gtrsim 10^{-3}\ M_\odot$ [76,77]. Using the ejecta of models $\{A1, A2, A3, A4\}$, and the fitting formulas provided in Ref. [78], we infer the peak time $\tau_{\rm peak}$ of the kilonova emission is $\{5.4, 4.6, 3.7, 5.2\}$ days, the peak luminosity $L_{\rm knova}$ of the ejecta is $\{1.3, 1.2, 2.1, 2.6\} \times 10^{40}$ ergs/s, and the effective temperature $T_{\rm peak}$ at the peak is $\{2.4, 2.6, 2.3, 2.1\} \times 10^3$ K, respectively. Significant ejecta are being created only from our rapidly rotating magnetars $A1$–$A4$, consistent with the suggestion that the magnetic field lines of a rotating compact object may accelerate fluid elements due to a magnetocentrifugal mechanism [79]. However, no highly collimated, helical magnetic fields or incipient jets, which are necessary for γ-ray bursts, arise at the poles of these magnetars by the time our simulations are terminated.

Discussion.—In this Letter we presented our latest GRMHD simulations of self-consistent, ultramagnetized equilibria. We constructed and evolved a diverse set of magnetars from slowly to rapidly rotating, most having mixed poloidal and toroidal magnetic fields of comparable strength. Although the specific geometry of the mixed field configuration can delay or accelerate the development of various well-known instabilities [39–41] all our models finally succumb to them. In addition, our initially uniformly rotating models develop differential rotation in their cores on a dynamical timescale, similar to that found in binary NS mergers. To establish exactly how differential rotation is spontaneously created requires further analysis. Our models (especially the rapidly rotating ones) exhibit large quasiradial oscillations in the NS's F mode, and produce significant amounts of ejecta that can power a kilonova. Our equilibria can be explored further with improved numerical evolution schemes that will address effects from the artificial atmosphere typically found in all ideal MHD simulations. In that direction one would employ the equations of resistive MHD in full GR [11,80–82] or a scheme that reliably matches GRMHD to its force-free limit [83]. Finally, the recent results by NICER [44,45] are calling for the development of solutions beyond the large scale dipolar magnetic field configurations. One important question is how do observed pulsars with their magnetic fields reach and maintain *uniform* rotation, which is believed necessary for pulsars to serve as very precise clocks? All of these matters will be the subject of our future explorations.

Movies highlighting results of our simulations can be found at [84].

We thank the Illinois Relativity REU team (H. Jinghan, M. Kotak, E. Yu, and J. Zhou) for assistance with some of the visualizations. This work has been supported in part by National Science Foundation (NSF) Grant No. PHY-2006066, and NASA Grant No. 80NSSC17K0070 to the University of Illinois at Urbana-Champaign, as well as by JSPS Grant-in-Aid for Scientific Research(C) 18K03624 to the University of the Ryukyus. This work made use of the Extreme Science and Engineering Discovery Environment (XSEDE), which is supported by National Science Foundation Grant No. TG-MCA99S008. This research is part of the Blue Waters sustained-petascale computing project, which is supported by the National Science Foundation (Awards No. OCI-0725070 and No. ACI-1238993) and the State of Illinois. Blue Waters is a joint effort of the University of Illinois at Urbana-Champaign and its National Center for Supercomputing Applications. Resources supporting this work were also provided by the NASA High-End Computing (HEC) Program through the NASA Advanced Supercomputing (NAS) Division at Ames Research Center. This research is part of the Frontera computing project at the Texas Advanced Computing Center. Frontera is made possible by National Science Foundation Award No. OAC-1818253.

*tsokaros@illinois.edu

[1] R. C. Duncan and C. Thompson, Astrophys. J. Lett. **392**, L9 (1992).
[2] C. Thompson and R. C. Duncan, Astrophys. J. **408**, 194 (1993).
[3] C. Thompson and R. C. Duncan, Astrophys. J. **473**, 322 (1996).
[4] A. K. Harding and D. Lai, Rep. Prog. Phys. **69**, 2631 (2006).
[5] C. Kouveliotou, S. Dieters, T. Strohmayer, J. van Paradijs, G. J. Fishman, C. A. Meegan, K. Hurley, J. Kommers, I. Smith, D. Frail, and T. Murakami, Nature (London) **393**, 235 (1998).
[6] F. P. Gavriil, V. M. Kaspi, and P. M. Woods, Nature (London) **419**, 142 (2002).
[7] D. Price and S. Rosswog, Science **312**, 719 (2006).
[8] M. Anderson, E. W. Hirschmann, L. Lehner, S. L. Liebling, P. M. Motl, D. Neilsen, C. Palenzuela, and J. E. Tohline, Phys. Rev. Lett. **100**, 191101 (2008).
[9] K. Kiuchi, P. Cerda-Durn, K. Kyutoku, Y. Sekiguchi, and M. Shibata, Phys. Rev. D **92**, 124034 (2015).
[10] K. Kiuchi, Y. Sekiguchi, K. Kyutoku, M. Shibata, K. Taniguchi, and T. Wada, Phys. Rev. D **92**, 064034 (2015).
[11] K. Dionysopoulou, D. Alic, and L. Rezzolla, Phys. Rev. D **92**, 084064 (2015).
[12] M. Shibata, M. D. Duez, Y. T. Liu, S. L. Shapiro, and B. C. Stephens, Phys. Rev. Lett. **96**, 031102 (2006).
[13] M. D. Duez, Y. T. Liu, S. L. Shapiro, M. Shibata, and B. C. Stephens, Phys. Rev. Lett. **96**, 031101 (2006).
[14] D. M. Siegel, R. Ciolfi, A. I. Harte, and L. Rezzolla, Phys. Rev. D **87**, 121302(R) (2013).

[15] T. W. Baumgarte, S. L. Shapiro, and M. Shibata, Astrophys. J. Lett. **528**, L29 (2000).
[16] S. L. Shapiro, Astrophys. J. **544**, 397 (2000).
[17] R. Aguilera-Miret, D. Viganò, F. Carrasco, B. Miñano, and C. Palenzuela, Phys. Rev. D **102**, 103006 (2020).
[18] B. P. Abbott *et al.* (Virgo, LIGO Scientific Collaborations), Phys. Rev. Lett. **119**, 161101 (2017).
[19] B. P. Abbott *et al.* (Virgo, Fermi-GBM, INTEGRAL, LIGO Scientific Collaborations), Astrophys. J. **848**, L13 (2017).
[20] S. Valenti, D. J. Sand, S. Yang, E. Cappellaro, L. Tartaglia, A. Corsi, S. W. Jha, D. E. Reichart, J. Haislip, and V. Kouprianov, Astrophys. J. **848**, L24 (2017).
[21] B. D. Metzger, T. A. Thompson, and E. Quataert, Astrophys. J. **856**, 101 (2018).
[22] M. Bocquet, S. Bonazzola, E. Gourgoulhon, and J. Novak, Astron. Astrophys. **301**, 757 (1995).
[23] K. Kiuchi and S. Yoshida, Phys. Rev. D **78**, 044045 (2008).
[24] K. Kiuchi, K. Kotake, and S. Yoshida, Astrophys. J. **698**, 541 (2009).
[25] C. Y. Cardall, M. Prakash, and J. M. Lattimer, Astrophys. J. **554**, 322 (2001).
[26] N. Yasutake, K. Kiuchi, and K. Kotake, Mon. Not. R. Astron. Soc. **401**, 2101 (2010).
[27] J. Frieben and L. Rezzolla, Mon. Not. R. Astron. Soc. **427**, 3406 (2012).
[28] D. Chatterjee, T. Elghozi, J. Novak, and M. Oertel, Mon. Not. R. Astron. Soc. **447**, 3785 (2015).
[29] B. Franzon, V. Dexheimer, and S. Schramm, Mon. Not. R. Astron. Soc. **456**, 2937 (2016).
[30] A. Pili, N. Bucciantini, and L. Del Zanna, Mon. Not. R. Astron. Soc. **439**, 3541 (2014).
[31] N. Bucciantini, A. G. Pili, and L. Del Zanna, Mon. Not. R. Astron. Soc. **447**, 3278 (2015).
[32] A. Pili, N. Bucciantini, and L. Del Zanna, Mon. Not. R. Astron. Soc. **470**, 2469 (2017).
[33] K. Kiuchi, M. Shibata, and S. Yoshida, Phys. Rev. D **78**, 024029 (2008).
[34] P. D. Lasky, B. Zink, K. D. Kokkotas, and K. Glampedakis, Astrophys. J. **735**, L20 (2011).
[35] R. Ciolfi, S. K. Lander, G. M. Manca, and L. Rezzolla, Astrophys. J. **736**, L6 (2011).
[36] P. D. Lasky, B. Zink, and K. D. Kokkotas, arXiv:1203.3590.
[37] R. Ciolfi and L. Rezzolla, Astrophys. J. **760**, 1 (2012).
[38] R. J. Tayler, Proc. Phys. Soc. London Sect. B **70**, 31 (1957).
[39] R. J. Tayler, Mon. Not. R. Astron. Soc. **161**, 365 (1973).
[40] G. A. E. Wright, Mon. Not. R. Astron. Soc. **162**, 339 (1973).
[41] P. Markey and R. J. Tayler, Mon. Not. R. Astron. Soc. **163**, 77 (1973).
[42] P. Markey and R. J. Tayler, Mon. Not. R. Astron. Soc. **168**, 505 (1974).
[43] E. Flowers and M. A. Ruderman, Astrophys. J. **215**, 302 (1977).
[44] M. Miller *et al.*, Astrophys. J. Lett. **887**, L24 (2019).
[45] T. E. Riley *et al.*, Astrophys. J. Lett. **887**, L21 (2019).
[46] K. Uryu, E. Gourgoulhon, C. Markakis, K. Fujisawa, A. Tsokaros, and Y. Eriguchi, Phys. Rev. D **90**, 101501(R) (2014).
[47] K. Uryu, S. Yoshida, E. Gourgoulhon, C. Markakis, K. Fujisawa, A. Tsokaros, K. Taniguchi, and Y. Eriguchi, Phys. Rev. D **100**, 123019 (2019).
[48] Z. B. Etienne, Y. T. Liu, and S. L. Shapiro, Phys. Rev. D **82**, 084031 (2010).
[49] See Supplemental Material at http://link.aps.org/supplemental/10.1103/PhysRevLett.128.061101 for details on the construction of the initial data and the simulations, which includes Refs. [50–65].
[50] K. Uryu, F. Limousin, J. L. Friedman, E. Gourgoulhon, and M. Shibata, Phys. Rev. D **80**, 124004 (2009).
[51] M. Shibata, K. Uryu, and J. L. Friedman, Phys. Rev. D **70**, 044044 (2004); **70**, 129901(E) (2004).
[52] E. Gourgoulhon, C. Markakis, K. Uryu, and Y. Eriguchi, Phys. Rev. D **83**, 104007 (2011).
[53] V. D. Shafranov, Sov. J. Exp. Theor. Phys. **6**, 545 (1958).
[54] H. Grad, Rev. Mod. Phys. **32**, 830 (1960).
[55] V. D. Shafranov, Rev. Plasma Phys. **2**, 103 (1966).
[56] J. L. Friedman and N. Stergioulas, *Rotating Relativistic Stars* (Cambridge University Press, Cambridge, England, 2013).
[57] M. Shibata and T. Nakamura, Phys. Rev. D **52**, 5428 (1995).
[58] T. W. Baumgarte and S. L. Shapiro, Phys. Rev. D **59**, 024007 (1998).
[59] Z. B. Etienne, J. A. Faber, Y. T. Liu, S. L. Shapiro, K. Taniguchi, and T. W. Baumgarte, Phys. Rev. D **77**, 084002 (2008).
[60] B. D. Farris, R. Gold, V. Paschalidis, Z. B. Etienne, and S. L. Shapiro, Phys. Rev. Lett. **109**, 221102 (2012).
[61] Z. B. Etienne, V. Paschalidis, Y. T. Liu, and S. L. Shapiro, Phys. Rev. D **85**, 024013 (2012).
[62] V. Paschalidis, M. Ruiz, and S. L. Shapiro, Astrophys. J. **806**, L14 (2015).
[63] M. Ruiz, R. N. Lang, V. Paschalidis, and S. L. Shapiro, Astrophys. J. **824**, L6 (2016).
[64] M. Ruiz, S. L. Shapiro, and A. Tsokaros, Phys. Rev. D **98**, 123017 (2018).
[65] M. Ruiz, A. Tsokaros, S. L. Shapiro, K. C. Nelli, and S. Qunell, Phys. Rev. D **102**, 104022 (2020).
[66] G. B. Cook, S. L. Shapiro, and S. A. Teukolsky, Astrophys. J. **422**, 227 (1994).
[67] A. Corsi and B. J. Owen, Phys. Rev. D **83**, 104014 (2011).
[68] K. Kashiyama and K. Ioka, Phys. Rev. D **83**, 081302(R) (2011).
[69] B. Zink, P. D. Lasky, and K. D. Kokkotas, Phys. Rev. D **85**, 024030 (2012).
[70] K. Uryu, A. Tsokaros, L. Baiotti, F. Galeazzi, K. Taniguchi, and S. Yoshida, Phys. Rev. D **96**, 103011 (2017).
[71] W. Kastaun and F. Galeazzi, Phys. Rev. D **91**, 064027 (2015).
[72] M. Hanauske, K. Takami, L. Bovard, L. Rezzolla, J. A. Font, F. Galeazzi, and H. Stöcker, Phys. Rev. D **96**, 043004 (2017).
[73] M. Ruiz, A. Tsokaros, and S. L. Shapiro, Phys. Rev. D **104**, 124049 (2021).
[74] J. N. Cook, S. L. Shapiro, and B. C. Stephens, Astrophys. J. **599**, 1272 (2003).
[75] J. L. Friedman, J. R. Ipser, and R. D. Sorkin, Astrophys. J. **325**, 722 (1988).
[76] L.-X. Li and B. Paczynski, Astrophys. J. Lett. **507**, L59 (1998).
[77] B. D. Metzger, Living Rev. Relativity **20**, 3 (2017).
[78] A. Perego, F. K. Thielemann, and G. Cescutti, *r*-process nucleosynthesis from compact binary mergers, in *Handbook*

of Gravitational Wave Astronomy, edited by C. Bambi (Springer, Singapore, 2021), p. 1.

[79] R. D. Blandford and D. G. Payne, Mon. Not. R. Astron. Soc. **199**, 883 (1982).

[80] C. Palenzuela, L. Lehner, O. Reula, and L. Rezzolla, Mon. Not. R. Astron. Soc. **394**, 1727 (2009).

[81] C. Palenzuela, Mon. Not. R. Astron. Soc. **431**, 1853 (2013).

[82] K. Dionysopoulou, D. Alic, C. Palenzuela, L. Rezzolla, and B. Giacomazzo, Phys. Rev. D **88**, 044020 (2013).

[83] V. Paschalidis and S. L. Shapiro, Phys. Rev. D **88**, 104031 (2013).

[84] http://research.physics.illinois.edu/cta/movies/SNS_2021/.